DENSITY FUNCTIONAL THEORY FOR TRAPPED ULTRACOLD FERMIONS

A THESIS SUBMITTED TO
THE GRADUATE SCHOOL OF NATURAL AND APPLIED SCIENCES
OF
MIDDLE EAST TECHNICAL UNIVERSITY

BY

ÖZGE AKYAR

IN PARTIAL FULFILLMENT OF THE REQUIREMENTS
FOR
THE DEGREE OF MASTER OF SCIENCE
IN
PHYSICS

AUGUST 2009

Approval of the thesis:

DENSITY FUNCTIONAL THEORY FOR TRAPPED ULTRACOLD FERMIONS

submitted by **ÖZGE AKYAR** in partial fulfillment of the requirements for the degree of **Master of Science in Physics Department, Middle East Technical University** by,

Prof. Dr. Canan Özgen _____
Dean, Graduate School of **Natural and Applied Sciences**

Prof. Dr. Sinan Bilikmen _____
Head of Department, **Physics**

Assist. Prof. Dr. Hande Toffoli _____
Supervisor, **Physics Department, METU**

Examining Committee Members:

Assoc. Prof. Dr. M. Özgür Öktel
Physics Dept., Bilkent University _____

Assist. Prof. Dr. Hande Toffoli
Physics Dept., METU _____

Prof. Dr. Mehmet Tomak
Physics Dept., METU _____

Prof. Dr. Şakir Erkoç
Physics Dept., METU _____

Assoc. Prof. Dr. Sadi Turgut
Physics Dept., METU _____

Date:26 August 2009

I hereby declare that all information in this document has been obtained and presented in accordance with academic rules and ethical conduct. I also declare that, as required by these rules and conduct, I have fully cited and referenced all material and results that are not original to this work.

Name, Last Name: ÖZGE AKYAR

Signature :

ABSTRACT

DENSITY FUNCTIONAL THEORY FOR TRAPPED ULTRACOLD FERMIONS

Akyar, Özge
M.S., Department of Physics
Supervisor : Assist. Prof. Dr. Hande Toffoli

August 2009, 32 pages

Recently a new outlook on dealing with dipolar ultracold fermions based on density functional methods has received attention. A Thomas-Fermi treatment coupled with a variational approach has been developed for a collection of fermions trapped in a harmonic potential interacting via dipole-dipole forces. In this thesis, firstly our alternative formalism for Thomas-Fermi method by performing some calculations based on the Kohn-Sham formalism which is one of the main idea of density functional theory is investigated. Furthermore, density distributions are obtained dependent to the parameters; rescaled interaction strength, dipole-dipole energy and the trap parameter which determine the trap geometry based on this theory. The thesis starts with a brief outline of the density functional theory and theory of our system, continues with calculations based on this theory, which are free of any variational assumptions for the density profile. Moreover, results of density graphics for harmonic trap will be followed by discussion of comparison and contrast with Thomas-Fermi method based on the paper of Goral *et al.*. These discussions are mainly about the shape of the density distribution, variation of the cloud parameters and energy behaviours according to the rescaled interaction strength. The thesis concludes with an analysis of

contribution of density functional theory to this fermionic system.

Keywords: ultracold fermions, density functional theory

ÖZ

TUZAKLANMIŞ ULTRASOĞUK FERMİYONLAR İÇİN YOĞUNLUK FONKSİYONELİ TEORİSİ

Akyar, Özge
Yüksek Lisans, Fizik Bölümü
Tez Yöneticisi : Yrd. Doç. Dr. Hande Toffoli

Ağustos 2009, 32 sayfa

Son dönemde yeni bir bakış açısı olan yoğunluk fonksiyoneli metodlarına dayalı olarak iki kutuplu ultrasoğuk fermiyonlarla uğraşmak oldukça ilgi çekiyor. Değişim yöntemi ile birleştirilmiş bir Thomas-Fermi yöntemi, iki kutuplu-iki kutuplu (dipol-dipol) kuvvetlerle etkileşen bir harmonik potansiyelde hapsedilmiş fermiyonlar toplamı için geliştirilmiştir. Bu tezde, öncelikle yoğunluk fonksiyoneli teorisinin ana fikirlerinden biri olan Kohn-Sham formalizmine dayalı olarak yapılan bazı hesaplamalarla Thomas-Fermi metoduna alternatif bir formalizm incelenmiştir. Buna ek olarak yeniden ölçeklendirilmiş etkileşim parametresi, iki kutup-iki kutup enerjisi, tuzak parametresine bağlı yoğunluk dagılımları elde edildi. Tez yoğunluk fonksiyoneli teorisinin ve sistemin teorisinin özet bir şekilde anlatımıyla başlar ve bu teoriye dayalı yoğunluk profili için herhangi bir değişkenden bağımsız hesaplamalarla devam etmektedir. Bundan başka, harmonik tuzak için yapılan yoğunluk grafiklerinin sonuçlarını, Goral grubunun makalesine dayalı olarak yapılan karşılaştırmalar ve tartışmalar izlemektedir. Bu tartışmalar temelde yoğunluk dağılımlarına, bulut parametrelerine ve ölçeklendirilmiş etkileşim parametresine göre incelenmiş enerjinin davranışına bağlıdır. Tez, yoğunluk fonksiyoneli teorisinin bu fermiyonik sisteme

katkılarının incelenmesiyle son bulmaktadır.

Anahtar Kelimeler: ultrasoğuk fermiyonlar, yoğunluk fonksiyoneli teorisi

To my family

ACKNOWLEDGMENTS

I would like to express my deepest gratitude and thanks to my supervisor Assist. Prof. Dr. Hande Toffoli for her guidance, help and patience. I also would like to thank my co-supervisor Assoc. Prof. Dr. M. Özgür Öktel for his valuable ideas, advice and supervision. Without their encouragement and support I would not have been able to complete this thesis.

I am also grateful to Assoc. Prof. Dr. Altuğ Özpineci for his encouragement at the beginning of my graduate life and willing to help me all the time.

I would like to thanks to my friends Engin, Türkan and Burak for their supports and beatiful friendship.

Finally, I would like to express my deepest thanks and appreciation to my family for their moral support and endless love during my entire life. And a special thanks goes out to Enderalp for his love, support and endless patience.

TABLE OF CONTENTS

LIST OF TABLES

TABLES

LIST OF FIGURES

FIGURES

CHAPTER 1

INTRODUCTION

Over the past decade, ultracold atoms have become very popular among quantum optics, atomic physics and solid state physics such that the observation of Bose-Einstein Condensation [1], [2], [3] has become the starting point. Those studies with both ultracold fermions and bosons composed the theoretical and experimental literature. Experimental literature have concentrated on trapped atoms by simply laser cooling of atoms [4]. There are several candidates for experiments to realize the dipolar quantum gas and the pioneering ones are Rydberg atoms [5] having a large electric dipole moment and Chromium atoms with a permanent magnetic dipole moment [6].

From a theoretical point of view, fermionic atoms present an interesting challenge since unlike the Coulombic case, their attraction can be attractive or repulsive depending on their orientation [7]. In other words when atoms are on top of each other, their interaction is attractive but when they are side by side the interaction is repulsive.

Previous treatments of the problem of ultracold atoms in a harmonic trap have mostly been carried within the Thomas-Fermi approximation [8]. The mostly analytical treatment of Goral *et al.* involves the solution of the resulting Thomas-Fermi equations via a two-parameter variational Gaussian density. The two parameters while providing much insight into the general size and aspect ratio of the resulting cloud, they do not account for the possibility of a non-Gaussian shape.

In this work, we adopt the two-parameter form of Goral *et al.* into a three-dimensional harmonic confinement potential and go beyond a prescribed form of the density and present a general density-functional treatment of the system by using Density Functional Theory.

This thesis is divided into four chapters. In the second chapter, the theoretical background of studied systems have been explained. In the third chapter, the construction of the Hamiltonain of the system and the performed calculations will be presented. In the last chapter, a brief summary of the thesis and the obtained results will be given.

CHAPTER 2

THEORETICAL BACKGROUND

2.1 Density Functional Theory

Density Functional theory is a strong quantum mechanical approach to the many body problem. The main idea is to determine the ground state properties of the many-body system via electronic density rather than many-body wave function by using functionals, which mean function of another function. DFT method is nowadays popular among solid state physics calculations.

2.1.1 Hohenberg-Kohn Theorems

Density functional theory is based on two theorems put forward by Hohenberg and Kohn [9]. The first theory basically states that for a given external potential $V_{ext}(\vec{r})$ in any interacting system, the ground state density $n(\vec{r})$ can be determined uniquely except for a constant. The proof is elementary and can be carried out by variational principle:
We assume a second external potential $V'_{ext}(\vec{r})$ which clearly differs from the other except by a constant with the groundstate wavefunction $\Psi'_{ext}(\vec{r})$ since it has a different $\hat{H}'_{ext}$ and Schrödinger equation but same ground state density, $n(\vec{r})$. Then if we write energies with the help of the minimal property of the ground state,

$$E' = \langle \Psi' | \hat{H}' | \Psi' \rangle < \langle \Psi | \hat{H}' | \Psi \rangle = \langle \Psi | \hat{H} + V'_{ext}(\vec{r}) - V_{ext}(\vec{r}) | \Psi \rangle \quad (2.1)$$

$$E' < E + \int [V'_{ext}(\vec{r}) - V_{ext}(\vec{r})]\, n(\vec{r}) dr \quad (2.2)$$

exchanging primed and unprimed variables gives,

$$E < E' + \int [V_{ext}(\vec{r}) - V'_{ext}(\vec{r})]\, n(\vec{r}) dr \tag{2.3}$$

Adding equations 2.2 and 2.3, we obtain

$$E + E' < E' + E \tag{2.4}$$

obviously gives us a contradiction.

The second theorem states that the functional $E[n]$ is universal and can be defined in terms of density $n(\vec{r})$ for any external potential $V(\vec{r})$. This density $n(\vec{r})$ that minimizes energy is the ground state density. The proof can again simply be illustrated.

As a starting point we write energy as a functional of $n(\vec{r})$

$$E[n] = T[n] + E_{int}[n] + \int V_{ext}(\vec{r}) n(\vec{r}) + E_{II} \tag{2.5}$$

where $T[n]$ is the kinetic energy, E_{II} is the interaction energy of the nuclei and E_{int} is the internal energy.

Then the first two terms can be written as the universal function $E[n]$, since kinetic and internal energies are only functionals of density.

$$E[n] = F[n] + \int V_{ext}(\vec{r}) n(\vec{r}) + E_{II} \tag{2.6}$$

Then the ground state energy is defined in terms of the ground state density $n(\vec{r})$ as

$$E = E[n] = \langle \Psi | \hat{H} | \Psi \rangle \tag{2.7}$$

Then by variational principle as in 1st theorem,

$$E = E[n] = \langle \Psi | \hat{H} | \Psi \rangle < \langle \Psi' | \hat{H} | \Psi' \rangle = E' \tag{2.8}$$

If we minimize the total energy with respect to $n(\vec{r})$, it gives us the exact ground state density.

2.1.2 Kohn-Sham equations

In 1965, Kohn and Sham [10] provided an approach for the results of Hohenberg-Kohn theorems with the orbitals instead of density and determine the exchange-correlation energy as a density functional. For an arbitrary $n(\vec{r})$, one can not give

an exact expression for $E_{xc}[n]$. However if we assume $n(\vec{r})$ is slowly varying, $E_{xc}[n]$ is approximated as;

$$E_{xc}[n] = \int n(\vec{r})\epsilon_{xc}(n(\vec{r}))d\vec{r} \tag{2.9}$$

where $\epsilon_{xc}(n(\vec{r}))$ is the exchange and correlation energy per electron of a uniform electron gas. This approximation is referred to as the local density approximation (LDA) [9]. In the Kohn-Sham formalism, the density is written in terms of an unspecified set of orbitals.

$$n(\vec{r}) = \sum_{i=1}^{N} |\psi_i(\vec{r})|^2 \tag{2.10}$$

where $\{\psi_i(\vec{r}\,')\}$ are referred to as the Kohn-Sham orbitals and N is the number of electrons. The total energy of this system can be written as

$$E = -\frac{1}{2}\sum_i \int \psi_i^* \nabla_i^2 \psi_i d\vec{r} + \int V_{ext}(\vec{r})n(\vec{r})d\vec{r} + \frac{1}{2}\int\int \frac{n(\vec{r})n(\vec{r}\,')}{|\vec{r}-\vec{r}\,'|}d\vec{r} + E_{xc}[n(\vec{r})] \tag{2.11}$$

as a functional of Kohn-Sham orbitals. To minimize the energy, we evaluate the variational derivative, $\frac{\delta E}{\delta \psi_i^*}$ of the total energy with respect to the orbitals since one can prove that it does not matter whether to take ψ_i, ψ_i^*, then set it equal to zero

$$\int \delta n(\vec{r}) \left\{ \phi(\vec{r}) + -\frac{1}{2}\nabla^2 + \mu_{xc}(n(\vec{r})) \right\} d\vec{r} = 0 \tag{2.12}$$

where

$$\phi(\vec{r}) = \upsilon_{ext}(\vec{r}) + \int \frac{n(\vec{r}\,')}{||\vec{r}-\vec{r}\,'||}d\vec{r}\,' \tag{2.13}$$

and

$$\mu_{xc}(n) = \frac{d[n\epsilon_{xc}(n)]}{dn} \tag{2.14}$$

Then one can find orbitals ψ_i that satisfy a system of one-particle Schrödinger equations by introducing Lagrange multipliers ϵ_i

$$\delta\left(E - \sum \epsilon_i \int |\phi_i|^2 d\vec{r}\right) = 0 \tag{2.15}$$

thus

$$\left\{ -\frac{1}{2}\nabla^2 + \phi(\vec{r}) + \mu_{xc}n(\vec{r}) \right\} \psi_i(\vec{r}) = \epsilon_i \psi_i(\vec{r}) \tag{2.16}$$

These equations are called as Kohn-Sham equations with the Kohn-Sham eigenvalues ε_i and have to be solved by self-consistenly.

2.2 Thomas-Fermi treatment

Thomas-Fermi [12, 13] treatment is a quantum mechanical solution of the many-body problem with the electronic density $n(\vec{r})$ variable that is mentioned as a precursor of density functional theory.

Thomas-Fermi energy which is a functional of density can be written as:

$$\begin{aligned} E_{TF}[n(\vec{r})] &= C_F \int [n(\vec{r})]^{5/3} d\vec{r} + \int n(\vec{r}) V_{ext}(\vec{r}) d\vec{r} \\ &+ \frac{1}{2} \iint \frac{n(\vec{r}) n(\vec{r}\,')}{|\vec{r} - \vec{r}\,'|} d\vec{r} d\vec{r}\,' \end{aligned} \tag{2.17}$$

This energy functional is formed by kinetic term, potential term and the Hartree-term respectively where the potential term can be varied according to the system. E_{TF} can be minimized under the constraint,

$$N = \int (d\vec{r}) n(\vec{r}) \tag{2.18}$$

where N is the total number of electrons and $d\vec{r}$ is the volume element.

Thomas-Fermi method has limited accuracy since it does not include exchange energy that is the conclusion of Pauli exclusion principle. Later on, Dirac [14] made a correction to the Thomas-Fermi theory by adding an exchange-energy for an uniform electric gas and this gives,

$$\begin{aligned} E_{TF}[n(\vec{r})] &= C_F \int [n(\vec{r})]^{5/3} d\vec{r} + \int n(\vec{r}) V_{ext}(\vec{r}) d\vec{r} \\ &+ \frac{1}{2} \iint \frac{n(\vec{r}) n(\vec{r}\,')}{|\vec{r} - \vec{r}\,'|} d\vec{r} d\vec{r}\,' + C_x \int [n(\vec{r})]^{4/3} d\vec{r} \end{aligned} \tag{2.19}$$

This form is referred to “Thomas-Fermi-Dirac theory”. However this Thomas-Fermi-Dirac theory still have an accuracy by the form of kinetic energy, exchange energy and by neglecting the electron correlation.

2.3 Ultracold Dipolar Fermions

Most of the theoretical and experimental challanges on molecular and atomic physics are based on ultracold weakly interacting dipolar quantum gases. In order to model

results of these studies, mostly mean-field theory and its extensions using Gross-Pitaevskii equation and Bogoliubov-de Gennes equations for bosons are used [15, 16, 17].

In Fermi gases of dipolar particles due to the Pauli exclusion principle, only the contribution of dipole-dipole effect is dominant since the short-range of interparticle distance is neglected. The dipole-dipole potential for these systems is

$$V_d(\vec{r}) = \frac{d^2}{r^3}(1 - 3\cos^2(\theta_r)) \tag{2.20}$$

where d characterizes the dipole moment, r is the interparticle distance and θ_r is the angle between the direction of the dipole moments and $\vec{r}$. This interaction is anisotropic and partially attractive and partially repulsive. Indeed when atoms are on top of each other ($\theta_r = 0$ or $\theta_r = 180$), they attract but when particles are side by side ($\theta_r = 90$) they repel each other as shown in Fig. 2.1. This anisotropy creates

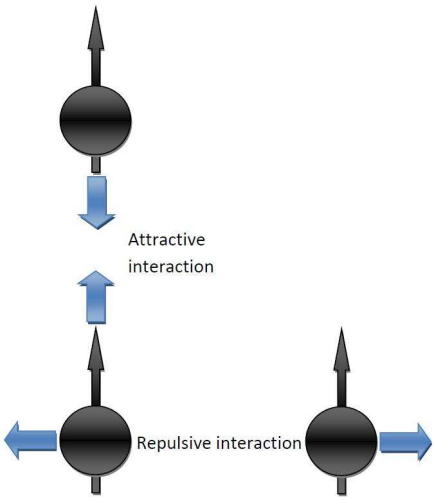

Figure 2.1: Dipole-dipole interaction

trap geometry that in a pancake trap ($\omega_\rho < \omega_z$) which is flat enough, the interaction is mainly repulsive and in an opposite situation that when they are in cigar shaped trap ($\omega_\rho > \omega_z$), particles are mainly repulsive.

In literature there are many studies with ultracold atoms. Review of ultracold dipolar

gases papers [7, 18, 19] and trapped atoms with dipolar interactions by S. Yi and L. You [20, 21] have been published in recent years. In Lewenstein *et al.* [19] paper, they work on shortly-weakly interacting trapped dipolar gases for both bosons and fermions and also observe ultracold dipolar gases in optical lattice. Another pioneering paper is published by Goral, Pfau and Rzazewski [22] and a Thomas-Fermi study by Goral group [8] which is our initiating point. In the paper of Goral *et al.* they employ semiclassical Thomas-Fermi theory to a dipole-dipole fermionic system in a harmonic trap and discuss the Dirac correction to this system. The harmonic trap is described by the potential

$$V_{trap} = \frac{1}{2} M\omega^2[x^2 + y^2 + (\beta z)^2] \tag{2.21}$$

where M is mass of the atomic species considered, ω is the trap frequency and β is trap parameter which describes the shape of trap. In their work, Goral *et al.* calculate the TFD energy through a Gaussian variational ansatz in a form

$$g(\vec{r}) \propto \kappa^3\gamma\, e^{[-\frac{1}{2}\kappa^2(x^2+y^2+\gamma^2z^2)]} \tag{2.22}$$

where κ is cloud size and γ is the aspect ratio for the density and a subsequent minimization. The ground state, together with several other properties are studied as a function of trap parameters.

The recent experimental results on dipolar quantum Bose gas of Chromium are studied by many groups [23, 24, 25] and realized important points about Bose Einstein Condensation of Chromium. In the paper of Griesmaier *et al.* [23] they realize the generation of Bose Einstein Condensation in a gas of Chromium atoms. The reason can be explained shortly with the large magnetic dipole moment property of Chromium. It has a very high magnetic moment ($6\mu_B$) since magnetic dipolar interaction is directly proportional with the square of magnetic moment, chromium makes it available to observe the dipole-dipole interaction in a quantum gas. The group got satisfactory results like observing BEC with 50.000 Cr atoms and determine temperature values.

CHAPTER 3

DESCRIPTION OF THE SYSTEM

3.1 Hamiltonian

The system studied in this work is a collection of fermions trapped in a harmonic potential interacting through a dipolar potential. The Hamiltonian is given as

$$\hat{H} = \hat{T} + \hat{V}_{dd} + \hat{V}_{ext} + \hat{V}_x \tag{3.1}$$

where $\hat{V}_{dd}$ is the dipolar potential between the particles, $\hat{V}_{ext}$ is the trap potential and $\hat{V}_x$ is the exchange part of the exchange-correlation potential which are to be explained in detail below. In this work we ignore the correlation potential. The dipolar part is,

$$\hat{V}_{dd}(\vec{r}, \vec{r}\,') = d^2 \frac{1 - 3\cos^2\theta}{|\vec{r} - \vec{r}\,'|^3} \tag{3.2}$$

where θ is the angle between the direction of dipolar moment and the vector of distance between the vectors $\vec{r}$ and $\vec{r}\,'$ and d is the dipole-dipole interaction strength. In our work, the direction of the dipolar moment is chosen as the z direction and all dipole moments are assumed to be aligned. The corresponding many-body Hamiltonian is

$$\hat{H} = \frac{-\hbar^2}{2m} \sum_i \nabla_i^2 + \frac{1}{2} d^2 \sum_{i \neq j} \frac{1 - 3\cos^2\theta_{ij}}{|\vec{r}_i - \vec{r}_j|^3} + \frac{1}{2} m\omega^2 \sum_i (x_i^2 + y_i^2 + \beta^2 z_i^2) \tag{3.3}$$

In order to get dimensionless variables the Hamiltonian is rescaled with the harmonic length

$$l = \sqrt{\frac{\hbar}{m\omega}} \tag{3.4}$$

to give

$$\tilde{\vec{r}} = \frac{\vec{r}}{l}, \quad \tilde{\vec{p}} = \frac{l\vec{p}}{\hbar} \tag{3.5}$$

since $[r_i, p_j] = i\hbar\delta_{ij}$ then these yield

$$[\tilde{r}_i, \tilde{p}_j] = i\delta_{ij}, \quad \tilde{p} = \frac{1}{i}\tilde{\delta} \tag{3.6}$$

finally the Hamiltonian in terms of the rescaled variables

$$\hat{H} = \sum_i \left(\frac{\hbar^2}{l^2} \frac{\tilde{p}_i^{\,2}}{2m} + \frac{1}{2} l^2 m\omega^2 \tilde{r}_i^{\,2} \right) + \frac{1}{2} d^2 \sum_{i \neq j} \frac{(1 - 3\cos^2\theta_{ij})}{l^3 |\tilde{\vec{r}}_i - \tilde{\vec{r}}_j|^3} \tag{3.7}$$

rearranging the Hamiltonian gives

$$\hat{H} = \sum_i \left(\hbar\omega \frac{\tilde{p}_i^{\,2}}{2} + \hbar\omega \frac{\tilde{r}_i^{\,2}}{2} \right) + \frac{1}{2} \frac{d^2}{l^3 \hbar\omega} \hbar\omega \sum_{i \neq j} \frac{(1 - 3\cos^2\theta_{ij})}{|\tilde{\vec{r}}_i - \tilde{\vec{r}}_j|^3} \tag{3.8}$$

and rescaling the energy by $\hbar\omega$

$$\frac{\hat{H}}{\hbar\omega} = \tilde{H} = \frac{1}{2} \sum_i [\tilde{\nabla}_i^{\,2} + \tilde{r}_i^{\,2}] + \frac{1}{2} \frac{d^2}{\frac{\hbar}{m\omega} \sqrt{\frac{\hbar}{m\omega}} \hbar\omega} \sum_{i \neq j} \frac{(1 - 3\cos^2\theta_{ij})}{|\tilde{\vec{r}}_i - \tilde{\vec{r}}_j|^3} \tag{3.9}$$

Finally we drop the tildes for simplicity

$$\hat{H} = \frac{1}{2} \sum_i \left[-\nabla_i^2 + x_i^2 + y_i^2 + \beta^2 z_i^2 \right] + \frac{1}{2} g \sum_{i \neq j} \frac{(1 - 3\cos^2\theta_{ij})}{|\vec{r}_i - \vec{r}_j|^3} \tag{3.10}$$

where

$$g = \frac{\mu_0 \mu^2}{4\pi} \frac{1}{l^3 \hbar\omega} \tag{3.11}$$

is the rescaled dipole-dipole parameter. As an example to check the correctness of rescaled parameter g, we take the example of Cr atoms which have a large magnetic dipole moment, μ of 6 Bohr magneton in a harmonic trap which has a frequency of $\nu = 10$ Hz in a recent experiment. In this study, for the calculation of rescaled interaction strength g, quantities are defined in Table 3.1.

Table 3.1: Rescaled parameters

Quality	Symbol	Value
Rescaled dipole strength	g	$\mu_0\mu^2/(4\pi l^3\hbar\omega)$
Permeability of vacuum	μ_0	$4\pi\ 10^{-17}$
Dipole moment of the atom	μ_B	$q_e\hbar/2m_e$
Frequency of the trap	ν	$10\ Hz$
Rescaled length	l	$\sqrt{\frac{\hbar}{m\omega}}$
Frequency of the trap	$\omega = 2\pi\nu$	$62.8Hz$

In Table 3.1, q_e is electron charge, m_e is electron mass. With our rescaling parameters, Cr which is among the species with the largest magnetic moment have a g of 17. With this value as our guide, we study a range of g values between 1 and 20 in order to cover all possible species. In our system, g has estimated as 7.66 with the variables given in Table 3.1. Finally we note that the parameter denoted by g in this work corresponds to ε

$$\varepsilon = (\omega M^3/\hbar^5)^{1/2}\frac{\mu_0}{4\pi}\mu^2 \tag{3.12}$$

in the work of Goral *et al.* [8] which helps to compare and contrast with this paper.
If we line up the differences between these two studies from a general look, in the Thomas-Fermi study the resulting figures are in restricted shapes however in this study we have no restriction. In addition, the Goral group made analytical calculations possible whereas this work is made up of completely numerical calculations. Finally they made possible of tunable parameters however our cloud shapes are not variable. Our Hamiltonian in Eq. 3.10 gives the total energy in the Kohn-Sham scheme as

$$E[n] = \frac{1}{2}\sum_i \int \psi_i^*(\vec{r})\nabla_i^2\psi_i(\vec{r})d\vec{r} + \frac{1}{2}\int d\vec{r}(x^2+y^2+\beta^2z^2)n(\vec{r}) + \frac{1}{2}g\int\int n(\vec{r})n(\vec{r}\,')\frac{(1-3\cos^2\theta)}{|\vec{r}-\vec{r}\,'|^3}d\vec{r}d\vec{r}\,' + E_x[n(\vec{r})] \tag{3.13}$$

where the density as defined earlier in Eq. 2.10 is

$$n(\vec{r}) = \sum_{i=1}^{N}|\psi_i(\vec{r})|^2 \tag{3.14}$$

In Eq. 2.16, we obtained Kohn-Sham equations. For our Hamiltonian, the energy equation Eq. 3.13 is minimized with respect to $\psi_i^*(\vec{r}\,')$ and the Kohn-Sham equations

are obtained as

$$\left[-\frac{1}{2}\nabla^2 + \frac{1}{2}m\omega(x^2+y^2+\beta^2z^2) + g\int \frac{n(\vec{r}')}{|\vec{r}-\vec{r}'|^3}(1-3\cos^2\theta) + V_x\right]\psi_i = \epsilon_i\psi_i \quad (3.15)$$

where the exchange potential

$$V_x(\vec{r}) = n(\vec{r})\,\frac{\partial\epsilon_x^{hom}(n)}{\partial n} + \epsilon_x^{hom}(n). \quad (3.16)$$

which is derived from local density approximation.

3.1.1 Basis Expansion

In order to solve the Kohn-Sham system of equations, a basis set in the form of

$$\psi_i(\vec{r}) = \sum_i f_i(\vec{r})C_{i\alpha} \quad (3.17)$$

has to be chosen as, where $f_i(\vec{r})$ are the basis functions and $C_{i\alpha}$ are the expansion coefficients. In calculations these bases sets can be chosen as plane-waves, Gaussian orbitals and wavelets [26]. This choice motivated by the fact that the first two terms of the Hamiltonian in Eq. 3.15 can be solved directly diagonal while the Hartree-like term of the Hamiltonian and the exchange energy part are evaluated numerically. The Hermite polynomials have two basic relationships [27] to facilitate the computational formation of the Hermite polynomial.

First one is the recursion relation that Hermite polynomial $H(x)$ satisfies

$$H_{n+1}(x) = 2xH_n(x) - 2nH_{n-1}(x) \quad (3.18)$$

and the other is the orthogonality integral

$$\int_{-\infty}^{\infty} H_m(x)H_n(x)e^{-x^2}\,dx = \delta_{nm} \quad (3.19)$$

The expansion of the Kohn-Sham orbitals include all Hermite polynomials up to a maximum total quantum number n_{max}

$$\phi_i(x) = \sum_n c_{i,n}u_n(x) \quad (3.20)$$

in one dimensional and when we skip to the three dimenional case, the Kohn-Sham orbitals become

$$\phi_i(\vec{r}) = \sum_{n_xn_yn_z}^{n_{max}} c_{i,n_x,n_y,n_z}u_{n_x}(x)u_{n_y}(y)u_{n_z}(\beta z) \quad (3.21)$$

where $u(x)$ is the Hermite function, $n = (n_x, n_y, n_z)$ and $n_x + n_y + n_z \leq n_{max}$. In the basis set representation, the above equations reduce to an eigenvalue equation

$$\bar{H}\bar{C} = \varepsilon\bar{C} \tag{3.22}$$

where

$$H = \begin{pmatrix} \langle\phi_1|\hat{H}|\phi_1\rangle & \langle\phi_1|\hat{H}|\phi_2\rangle & \cdots & \langle\phi_1|\hat{H}|\phi_n\rangle \\ \langle\phi_2|\hat{H}|\phi_1\rangle & \langle\phi_2|\hat{H}|\phi_2\rangle & \cdots & \langle\phi_1|\hat{H}|\phi_n\rangle \\ \vdots & \vdots & \ddots & \vdots \\ \langle\phi_n|\hat{H}|\phi_1\rangle & \langle\phi_n|\hat{H}|\phi_2\rangle & \cdots & \langle\phi_n|\hat{H}|\phi_n\rangle \end{pmatrix}$$

The kinetic and trap terms immediately yield

$$\langle\phi_n|\hat{T} + \hat{V}_{trap}|\phi_m\rangle = H_{nm} = \delta_{n_x m_x}\delta_{n_y m_y}\delta_{n_z m_z}(n_x + n_y + n_z + \frac{3}{2}) \tag{3.23}$$

where $n = (n_x, n_y, n_z)$ and $m = (m_x, m_y, m_z)$ are understood to be combined indices. For the Hartree integral which is of the form

$$\int d\vec{r}\frac{n(\vec{r}')}{|\vec{r} - \vec{r}'|^3}(1 - 3\cos^2\theta)H_i(\vec{r})H_j(\vec{r}) \tag{3.24}$$

is evaluated numerically on a one(and then three) dimensional grid. This potential needs a cutoff radius to avoid singularities. In order to assess the effect of the value of this cutoff a series of test calculations for different cutoff radii were performed. In these calculations, the factor g was taken to be 10 and the number of Hermite polynomials was taken to be 8 . The results are presented in Table 3.2. For our production runs, we take $r_{cut} = 0.5$ which is the smallest value of r_{cut} that gives us a converged result. This cutoff makes a difference in the Hartree term as shown in Fig. 3.1

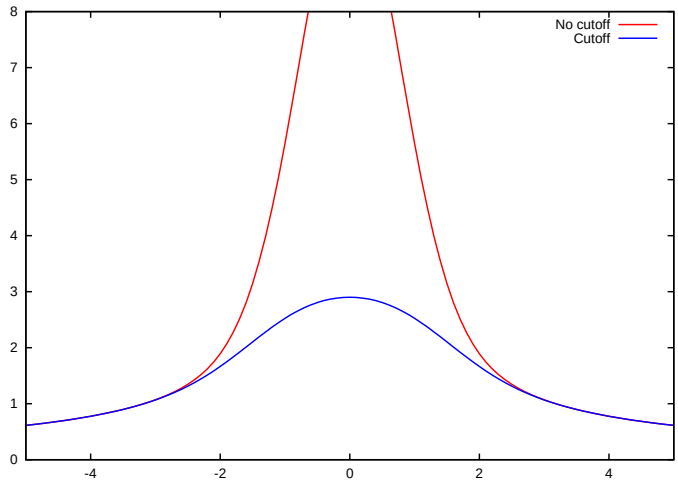

Figure 3.1: Cutoff for the Hartree term

After putting a cutoff value the Hartree-like term is evaluated numerically just because $(1 - 3\cos^2\theta)$ term only gives us a constant.

The Kohn-Sham equations in Eq. 2.16 in matrix form are solved self-consistently, which means the density obtained from the calculation is again placed into the starting point and this loop continues until the density is consistent with itself. At each step the lowest number of electrons in the Kohn-Sham levels are populated and the sum in Eq.2.10 is evaluated over these populated states. However this density is not used directly as a result, it is used along with a simple mixing scheme to update the density at step number $i + 1$,

$$n_{i+1}(\vec{r}) = \alpha n_i(\vec{r}) + (1 - \alpha)n_{i+1}(\vec{r}) \tag{3.25}$$

with $0 < \alpha < 1$ in order to ensure nonoscillatory convergence. The $alpha$ value used in our system is 0.4

3.1.2 Exchange energy

The exchange part of the Hamiltonian can be calculated with a second quantized Hamiltonian study with the perturbation theory. First the aim is to find the ground state energy of the system that has a uniform density n. We begin by taking the Fourier transform of the dipolar potential. It is easier to take the Fourier transform of

$\partial_z^2 \frac{1}{r}$ rather then interaction potential since we realize

$$\frac{1 - 3\cos^2\theta}{r^3} = -\partial_z^2 \frac{1}{r} \tag{3.26}$$

Now the next step is taking the Fourier transform of $-\partial_z^2 \frac{1}{r}$ which can be calculated by the general Fourier transform rules

$$V_{\vec{q}} = d^2 \frac{4\pi q_z^2}{q^2}, q \neq 0 \tag{3.27}$$

where d characterizes the dipole interaction strength, q_z is the z-component og Fourier variable and $q = 0$ component already equals zero since the average of the dipole potential over any spherical shell is zero. Using this, we write the second quantized Hamiltonian as

$$\hat{H} = \hat{H}_0 + \hat{H}_1 \tag{3.28}$$

where $\hat{H}_0$ is the unperturbed Hamiltonian which represents the noninteracting system and $\hat{H}_1$ is the (small) perturbed one. In second quantization representation

$$\hat{H} = \sum_{\vec{k}} \frac{\hbar^2 k^2}{2m} a^\dagger_{\vec{k}} a_{\vec{k}} + \frac{4\pi d^2}{2V} \sum_{\vec{k_1},\vec{k_2},\vec{q}} \frac{q_z^2}{q^2} a^\dagger_{\vec{k_1}+\vec{q}} a^\dagger_{\vec{k_2}-\vec{q}} a_{\vec{k_2}} a_{\vec{k_1}} \tag{3.29}$$

where V is the volume of the system, $\vec{k}'s$ are the wavenumbers and $a, a^\dagger$ are the fermionic creation and annihilation operators.

To facilitate the perturbative description we seek to identify a dimensionless parameter. We start with the dipolar Bohr radius

$$a_0 = \frac{\hbar^2}{md^2} \tag{3.30}$$

and the interparticle distance r_0 define in terms of the volume of the system

$$V = \frac{4}{3}\pi r_0^3 N \tag{3.31}$$

where $\frac{N}{V} = n = constant$, thus

$$r_0 = n^{-1/3} \left(\frac{3}{4\pi}\right)^{1/3} \tag{3.32}$$

The ratio of these two quantities gives us the dimensionless measure of the dipole interaction

$$r_s = \frac{r_0}{a_0} \tag{3.33}$$

where clearly large r_s gives the non-interacting limit. The first order energy shift is

$$\begin{aligned} E^{(1)} &= \langle F|\hat{H}_1|F\rangle \\ &= -\frac{d^2}{2V}\sum_{k,q}\frac{4\pi}{q^2}q_z^2\theta(k_f-|k+q|)\theta(k_f-k) \\ &= -\frac{d^2}{2}\frac{4\pi V}{(2\pi)^6}2\int d^3k\, d^3q\, q^{-2}\cos^2\theta\, q^2\, \theta(k_f-|k+q|)\,\theta(k_f-k) \end{aligned} \quad (3.34)$$

In the above equation $|F\rangle$ is the normalized ground state, $\hat{H}_1$ is the small perturbed Hamiltonian mentioned before and in addition $V/(2\pi)^3$ term comes from turning sum to the integral, 2 factor arises from the spin sum and q_z is replaced by $q\cos\theta$. Furthermore in Eq. 3.34 the Heaviside step function, $\theta(x)$ is used since the Pauli exclusion principle allows that only two fermions, one with spin-up and one with spin-down in each momentum eigenstate and the ground state $|F\rangle$ is obtained by filling the states up to k_f. In other words, the first-order energy shift, $E^{(1)}$ only survives when $k_f > k$. Then the integral becomes with the volume elements

$$E^{(1)} = -d^2\frac{4\pi V}{(2\pi)^6}\int d^3k\, d^3q\cos^2\theta\,\theta(k_f-|k+q|)\theta(k_f-k) \quad (3.35)$$

It is convenient to change variables from $\vec{k}$ to $\vec{P} = \vec{k} + \frac{1}{2}\vec{q}$ to reduce the Eq. 3.35 into a symmetrical form

$$E^{(1)} = -d^2\frac{4\pi V}{(2\pi)^6}\int\cos^2\theta\, d^3q\int d^3P\,\theta\left(k_f-|\vec{P}+\frac{1}{2}\vec{q}|\right)\theta\left(k_f-|\vec{P}-\frac{1}{2}\vec{q}|\right) \quad (3.36)$$

The evaluation of

$$\int d^3P\,\theta\left(k_f-|\vec{P}+\frac{1}{2}\vec{q}|\right)\theta\left(k_f-|\vec{P}-\frac{1}{2}\vec{q}|\right) \quad (3.37)$$

can be solved from the simple problem in geometry [28]. The step functions in the integrals give us restrictions as

$$\theta\left(k_f-|\vec{P}-\frac{1}{2}\vec{q}|\right) = \begin{cases} 1 & \text{if } k_f > |\vec{P}+\frac{1}{2}\vec{q}|; \\ 0 & \text{if } k_f < |\vec{P}+\frac{1}{2}\vec{q}|. \end{cases}$$

and same as the other one, thus for a nonvanishing integral there must be an intersecting volume for this integral like in Fig. 3.2.

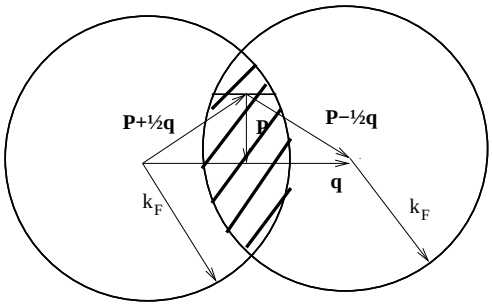

Figure 3.2: Intersection of two spheres

From now on the integral turns to volume of an intersecting two spheres and easy to calculate. This well known problem, “Intersection of two spheres” has a solution [29] like

$$V = \frac{1}{12}\pi(4R + d)(2R - d)^2 \tag{3.38}$$

this is the case of $r = R$ where r and R are the radii of the spheres. Thus, we imply the volume equation into our problem and the integral in Eq. 3.37 turns into

$$\int d^3P\ \theta\left(k_f - |\vec{P} + \frac{1}{2}\vec{q}|\right)\theta\left(k_f - |\vec{P} - \frac{1}{2}\vec{q}|\right) = \frac{4\pi}{3}k_f^3\left(1 - \frac{3}{2}x + \frac{1}{2}x^3\right)\theta(1 - x) \tag{3.39}$$

where $x = \frac{q}{2k_f}$. The first order energy shift integral is now elementary

$$E^{(1)} = -d^2\frac{(4\pi)^2V}{(2\pi)^6}\frac{k_f^3}{3}\int_0^1\int_{-\pi}^{\pi}\cos^2\theta\ q^2\ dq\ \sin\theta\ d\theta\ d\phi\left(1 - \frac{3}{2}x + \frac{1}{2}x^3\right) \tag{3.40}$$

and evaluating the cosine integral

$$E^{(1)} = -d^2\frac{4V}{(2\pi)^3}\frac{k_f^3}{3}\frac{-2}{3}\int q^2\ dq\left(1 - \frac{3}{2}x + \frac{1}{2}x^3\right) \tag{3.41}$$

In the above part x was determined as $x = \frac{q}{2k_f}$, thus

$$q = 2k_f x,\ \ dq = 2k_f\ dx \tag{3.42}$$

and so energy integral becomes

$$E^{(1)} = -d^2\frac{V}{(2\pi)^3}\frac{8}{9}k_f^3\int_0^1 4k_f^2\ 2k_f\ dx\left(1 - \frac{3}{2}x + \frac{1}{2}x^3\right) \tag{3.43}$$

The above integral simply gives the result

$$E^{(1)} = -\frac{d^2V}{\pi^3}\frac{1}{27}k_f^6 \tag{3.44}$$

In order to do a perturbation series in $1/r_s$, the maximum Fermi wavenumber k_f must be written in terms of r_s and it can be determined by computing the expectation value of the number operator in the ground state $|F\rangle$ as it is done in [**?**]

$$\begin{aligned} N &= \langle F|\hat{N}|F\rangle = \sum_k \langle F|\hat{n}_k|F\rangle = \sum_k \theta(k_f - k) \\ &= \frac{V}{(2\pi)^3}\sum_k \int d^3k\theta(k_f - k) \end{aligned} \tag{3.45}$$

which yields

$$N = \frac{V}{3\pi^2}k_f^3 \Rightarrow k_f = \left(\frac{3\pi^2 N}{V}\right)^{1/3} \tag{3.46}$$

From Eq. 3.32 now it is possible to write k_f in terms of r_0

$$k_f = \left(\frac{9\pi}{4}\right)^{1/3}\frac{1}{r_0} \tag{3.47}$$

If we return back to the Eq. 3.44 and place the k_f variable into this equation, it gives an elementary first order energy shift result

$$E^{(1)} = \frac{d^2}{r_0 a_0^6}\left(\frac{1}{r_s}C_2\right) \tag{3.48}$$

where $C_2 = -\dfrac{16}{3\pi}$

3.1.3 Preliminary results

In this study, convergence tests were conducted with respect to the cutoff radius and the basis sets. The dipole-dipole energy were analytically calculated for a normalized Gaussian distribution of unit width for a set of cutoff radii and data are token as

Table 3.2: cutoff radius values

r_{cut}	E_{dd}
0.2	0.8397
0.3	0.6017
0.4	0.5769
0.5	0.5729
0.6	0.5470
0.7	0.5054

As seen in Table 3.2 a cutoff radius of 0.5 length units yield a good compromise between a rapidly changing potential near the origin and one that is unrealistically smooth and was chosen as a fixed cutoff value for all the following calculations. This conclusion stems from the fact that around $r_{cut} = 0.5$ there is a window of values for which the dipole-dipole energy does not change appreciably. For r_{cut} larger than 0.5, the energy begins to deteriorate due to a potential that does not represent the Coulombic one accurately.

The basis set used to expand the Kohn-Sham orbitals involves a number of total $n = n_x + n_y + n_z$ of Hermite polynomials. Convergence of the total energy was checked up to $n_{max} = 10$. Sufficient convergence was achieved for $n_{max} = 8$ and for cutoff radius for the total energy as shown below

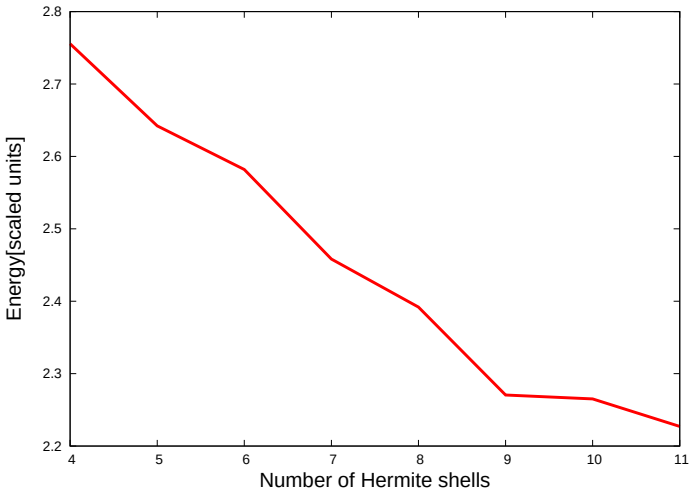

Figure 3.3: Total energy convergence with respect to N_g with $r_{cut} = 0.5$ and $g = 2.0$

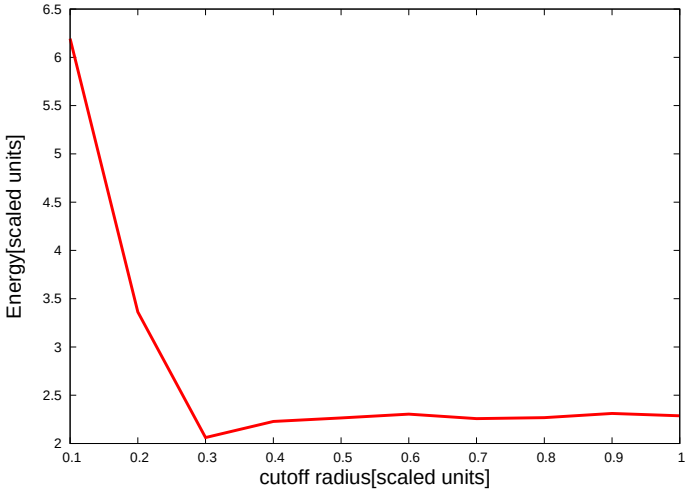

Figure 3.4: Total energy convergence with respect to cutoff with $N_g = 10$ and $g = 2.0$

After the preliminary discussions and studies, results based on the density profiles are obtained first in one dimension. For rather small numbers of electrons comparing with the three dimension studies, we plot Fig. 3.5(a) and Fig. 3.5(b) for 2 electrons with 12 Hermite polynomials which is an enough number of basis vectors for showing the density profile and plot Fig. 3.6(a), Fig. 3.6(b) for 5 electrons with 12 Hermite polynomials.

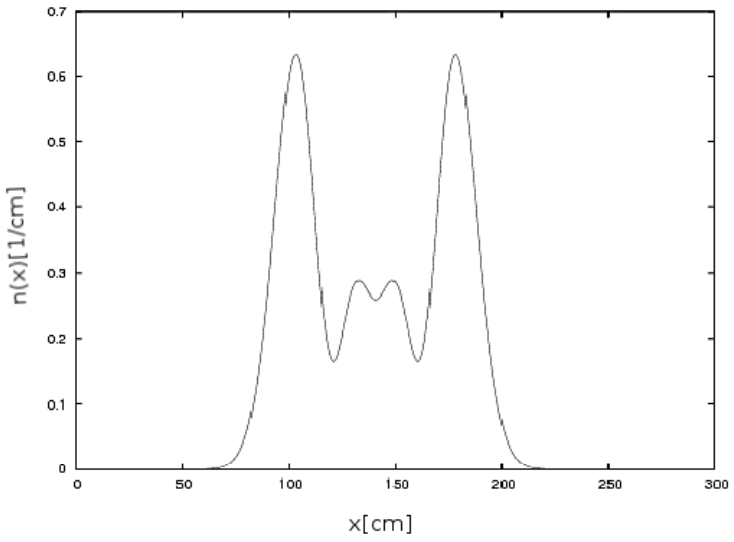

(a) g=0.01

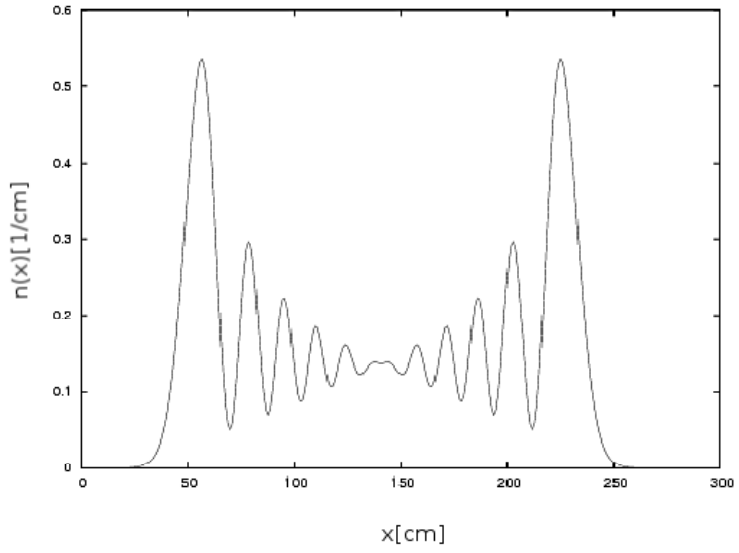

(b) g=0.8

Figure 3.5: 1D density graphs for $N_e = 2$

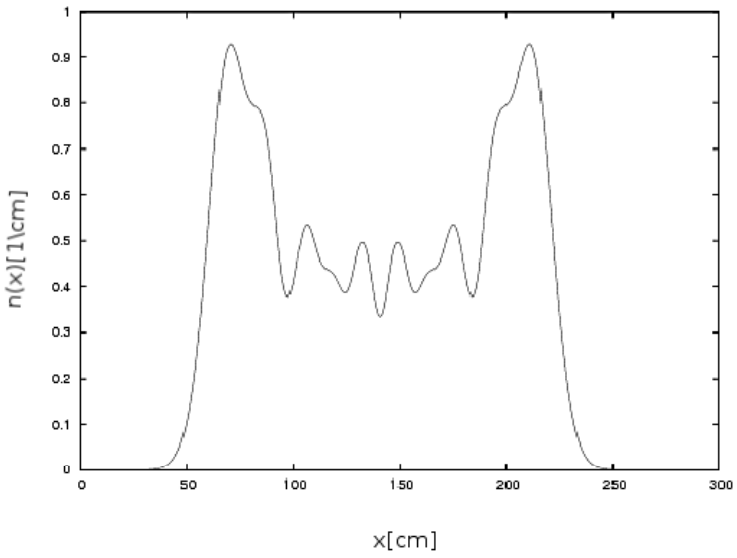

(a) g=0.01

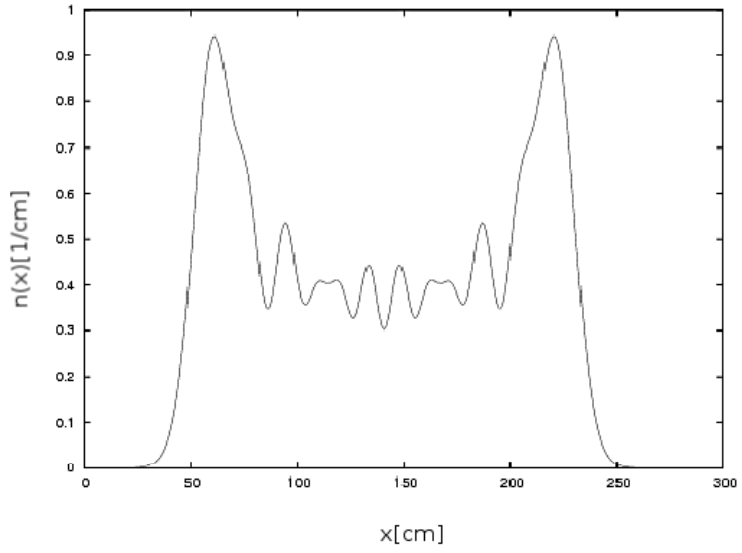

(b) g=0.8

Figure 3.6: 1D density graphs for $N_e = 5$

For the three dimensionel case, we both plot figures for different values of interaction and particle number for trap aspect ratio $\beta = 1$ which is the symmetric case as in the form of contour plots and cloud shapes. In Fig. 3.7 and Fig. 3.8, contour plots are plotted for $N_e = 2$, $N_e = 5$ and $N_e = 40$ which are ideal quantities for observing the difference for the rescaled dipolar strength parameter $g = 1$, $g = 3$ and $g = 40$ respectively. Along with the increase in rescaled dipole-dipole strength parameter g from 1 to 19, it can be observed that dipolar atoms which are chosen to be parallel in our study, repel each other as expected and mentioned in Sec. 2.3. However for the small numbers of electrons there is not a Gaussian distribution like shape, rather an hourglass-shaped one.

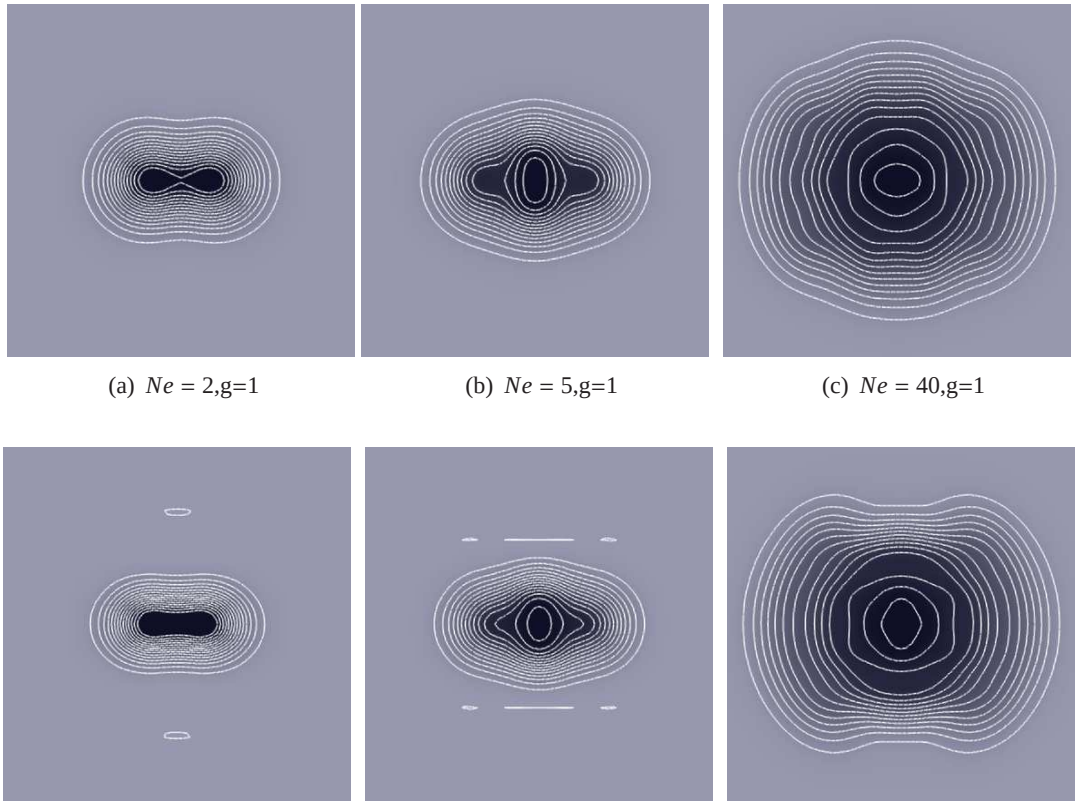

(a) Ne = 2,g=1 (b) Ne = 5,g=1 (c) Ne = 40,g=1

(d) Ne = 2,g=3 (e) Ne = 5,g=3 (f) Ne = 40,g=3

Figure 3.7: A few ground state density contour plots for different values of particle number with $g = 1$ and $g = 3$ for trap aspect ratio $\beta = 1$.

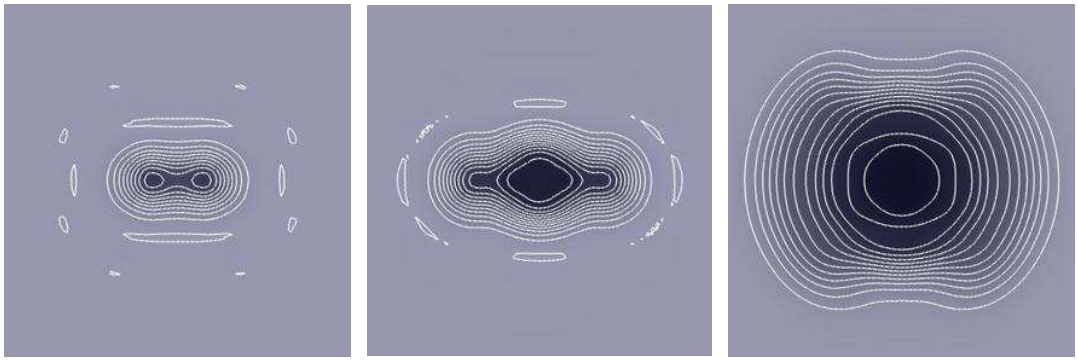

(a) Ne = 2,g=19 (b) Ne = 5,g=19 (c) Ne = 40,g=19

Figure 3.8: A few ground state density contour plots for different values of particle number and with $g = 19$ for trap aspect ratio $\beta = 1$.

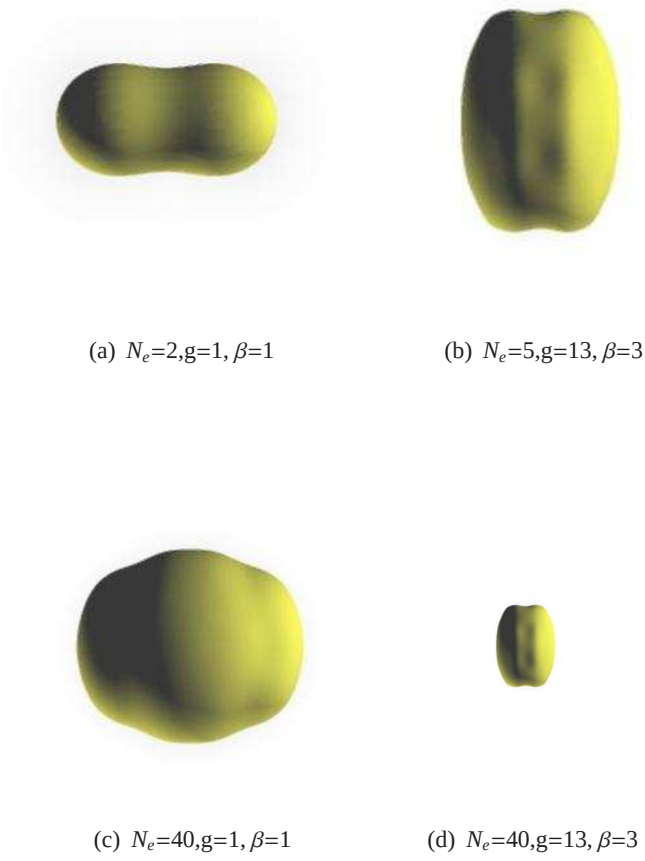

(a) N_e=2,g=1, β=1 (b) N_e=5,g=13, β=3

(c) N_e=40,g=1, β=1 (d) N_e=40,g=13, β=3

Figure 3.9: A few ground state density cloud shapes for different values of interaction, particle number and tcutoff radii and data are token as rap aspect ratio.

For the whole picture of the contour plots which are in the form of clouds in Fig. 3.9, it is more difficult to observe the density profiles rather than contour plots. The above figures are again for the numbers of particles and dipole strengths but now for different aspect ratios.

Furthermore in addition to these figures, we do some comparison tests in order to check the reliability of this study by plotting the figures in the work of Goral *et al.* which is mentioned in Sec. 2.3. All those figures below are plotted depending on the relation between the ε in Eq. 3.12 and the g factor mentioned in the paper of Goral *et al.* [8] in FIG.4.

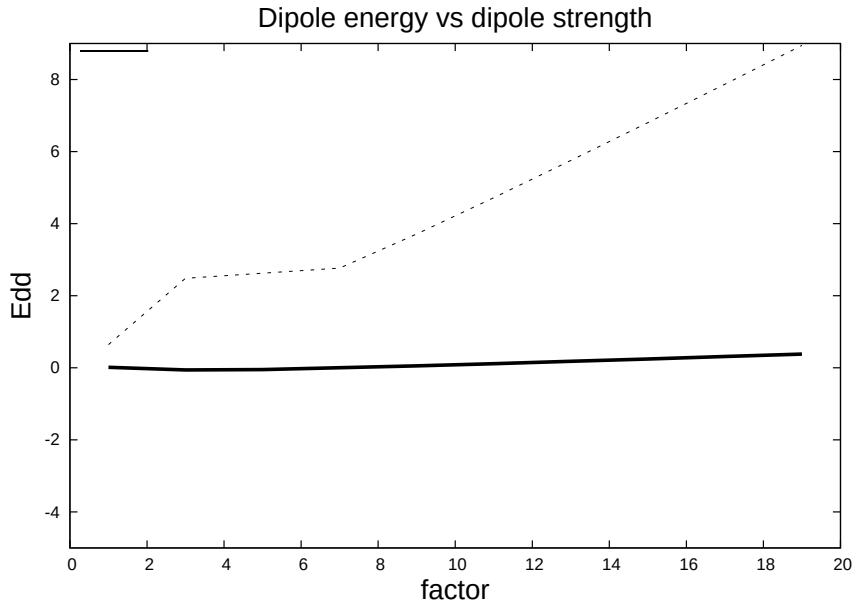

(a) N_e=2

Figure 3.10: Dipole-dipole interaction energy E_{dd} as a function of the interaction strength g for number of electrons $N_e = 2$. The solid line is for trap aspect ratio $\beta = 1$ and the dashed line is for trap aspect ratio $\beta = 3$.

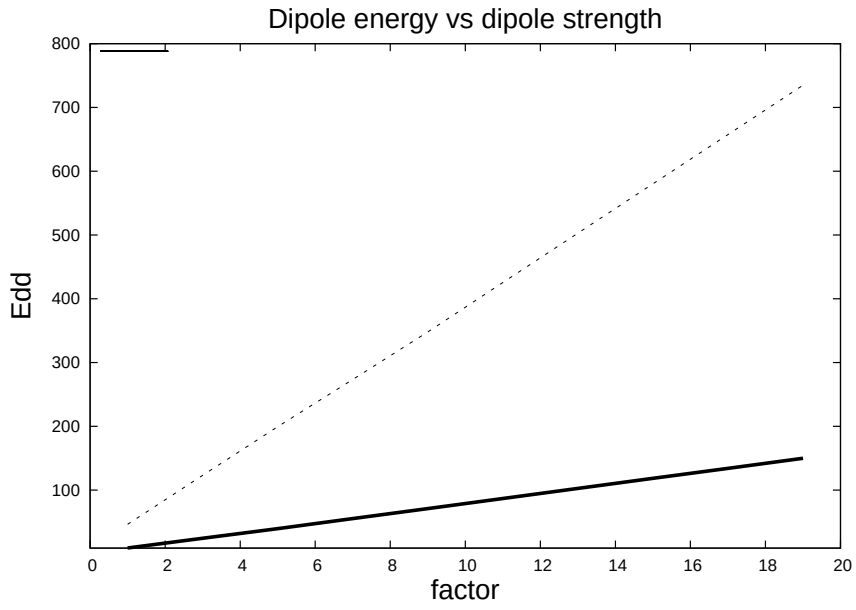

(a) N_e=40

Figure 3.11: Dipole-dipole interaction energy E_{dd} as a function of the interaction strength g for number of electrons $N_e = 40$. The solid line is for trap aspect ratio $\beta = 1$ and the dashed line is for trap aspect ratio $\beta = 3$.

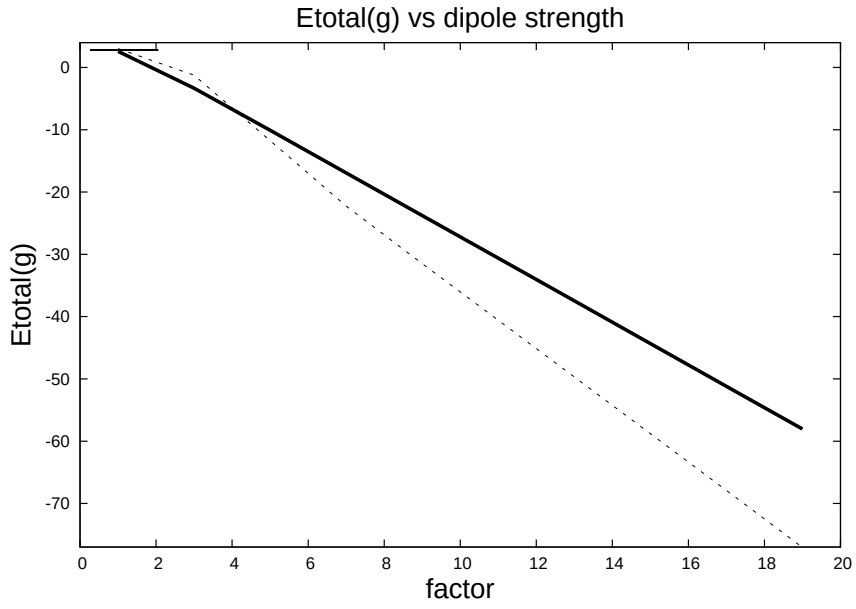

(a) N_e=2

Figure 3.12: Total energy E_T as a function of the interaction strength g for number of electron $N_e = 2$. The solid line is for trap aspect ratio $\beta = 1$ and the dashed line is for trap aspect ratio $\beta = 3$.

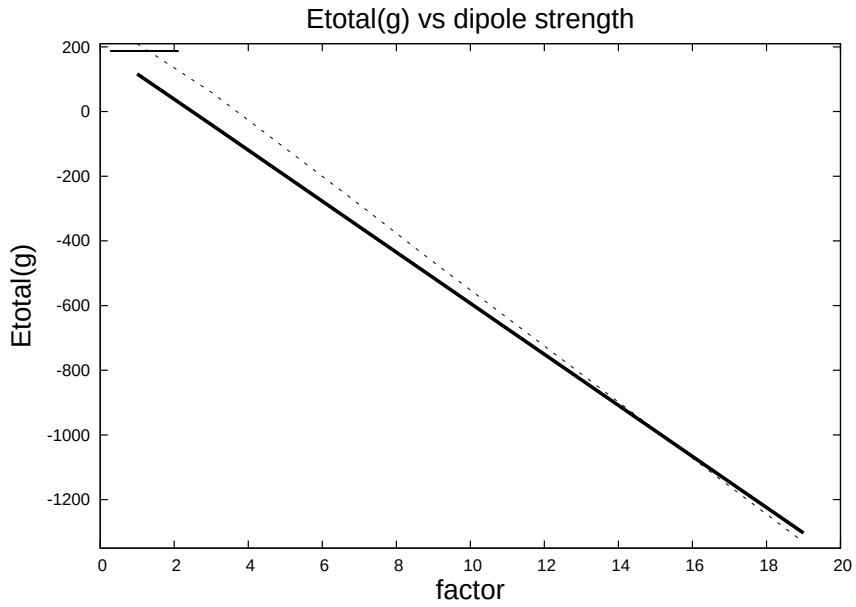

(a) N_e=40

Figure 3.13: Total energy E_T as a function of the interaction strength g for number of electron $N_e = 40$. The solid line is for trap aspect ratio $\beta = 1$ and the dashed line is for trap aspect ratio $\beta = 3$.

In order to see the behaviour of dipole-dipole energy in terms of rescaled dipole-dipole strength, we figured it for different numbers of electrons as shown in the Fig. 3.10 and Fig. 3.11. For these two figures, one can say that the increase of the E_{dd} with the increasing dipole-dipole interaction can not be observed easily in Fig. 3.10 according to Fig. 3.11 since the electron number is not satisfying enough. However, in Figure 3.11 the bigger the dipole-dipole strength factor, the bigger the dipole-dipole energy as expected. On the other hand for s special case of trap aspect ratio β, that if its value is large enough, E_{dd} will turn out to negative values except some critical points. The reason is for the large values, the trap becomes a prolate trap and the attraction dominates the trap because of the position of the particles mentioned in Sec. 2.3.

Furthermore, we take a look at the total energy, in terms of the rescaled dipole-dipole strength as figured out in Fig. 3.12 and Fig. 3.13. It can be observed that that there is an decreasing energy with increasing g parameter since in our system the exchange energy is a dominant factor which has a negative value and affect the whole energy in

this way.

Finally, we look at the normalized total energy which means that total energy divided by the non-interacting dipole-dipole energy as shown in Fig. 3.14 and observe that the non-interacting energy has a direct behaviour with the total energy.

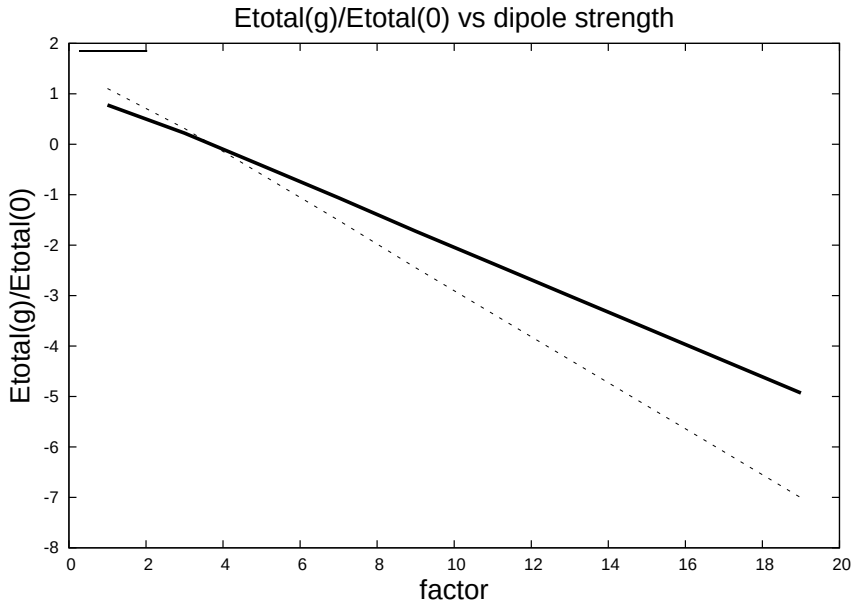

Figure 3.14: Normalized total energy as a function of the interaction strength g for number of electron $N_e = 40$. The solid line is for trap aspect ratio $\beta = 1$ and the dashed line is for trap aspect ratio $\beta = 3$

CHAPTER 4

CONCLUSION

In this thesis, we studied ultracold dipolar fermions in a harmonic trap and analyze the behaviour of the density. In this work, different from the other ultracold atom studies, a density functional treatment has been investigated. Calculations for the exchange energy of the dipolar fermions show that the exchange term is very large and unlike Coulombic systems it is mostly responsible for the behaviour of the system. For instance, in the absence of the exchange energy and for $\beta > 1$, the density cloud is seen to collapse into a very narrow disc and inclusion of the exchange effectively pushes electrons apart countering the flattening. In addition, the correlation part of the Hamiltonian has been ignored in this work.

The fermionic atoms different from the Coulombic case, show repulsive property in the dipole-dipole energy and total energy graphs where both energies are figured out as a function of the interaction strength as expected since the dipolar atoms are chosen to be parallel. For the dipole-dipole energy, it shows an increasing trend because of the increasing effect of dipolar strength. However for the total energy case with the dominance of exchange energy it has an decreasing trend as a function of rescaled dipole-dipole parameter.

For a small number of electrons, we get an hourglass-shaped density profile which is quite far from the Gaussian expectations. However, for larger numbers of electrons the density assumes the form of a large ellipsoidal cloud recovering partially the Gaussian-like shape.

The aim of this thesis is to propose an alternative formalism to Thomas-Fermi treatment to the work of Goral *et al.*. We adopt the two-parameter form of external potential energy of the harmonic trap of paper into a three-dimensional form, occur a

common unitless interaction strength term and plot efficacious figures for the comparison and contrast with their study. In the light of obtained results from the density functional theory calculations, we get density distributions with non-restricted shape contrary to the paper of Goral group.

REFERENCES

[1] H.M. Anderson, J.R. Ensher, M.R. Matthews, C.E. Wieman, and E.A. Cornell, Science 269, 198 (1995).

[2] C.C. Bradley, C.A. Sackett, J.J. Tollett, and R.G. Hulet, Phys. Rev. Lett. 75, 1687 (1995).

[3] K.B. Davis, M.-O. Mewes, M.R. Andrews, N.J. van Druten, D.S. Durfee, D.M. Kurn, and W. Ketterle,Phys. Rev. Lett. 75, 3969 (1995).

[4] C. Pethick and H. Smith, Bose-Einstein Condensation in Dilute Gases (Cambridge University Press, 2002)

[5] T.F. Gallagher, Rydberg Atoms (Cambridge University Press, 1994).

[6] A. Griesmaier, J. Phys. B 40, 91 (2007).

[7] M. Baranov, L. Dobrek, K. Goral, L. Santos, and M. Lewenstein, Physica Scripta 102, p. 74 (2002).

[8] Goral K., Englert B.-G., Rzazewski K., Phys. Rev. 63, A033606, (2001).

[9] Hohenberg, P., Kohn, W., Phys. Rev. 136, B864 (1964).

[10] Kohn, W., Sham, L.J., Phys. Rev. 140, A1133 (1965).

[11] Martin R. M., “Electronic Structure”, (Cambridge University Press, 2004).

[12] Thomas, L., H., Proc. Cambridge Philos. Soc. 23, 542, (1926).

[13] Fermi E., Rend. Lincei 6, 602 (1927).

[14] P. A. M. Dirac, Proc. Cambridge Philos. Soc. 26, 376, (1930).

[15] Dalfovo, F., Giorgini, S., Pitaevskii L. P., and Stringari, S., Rev. Mod. Phys. 71, 463 (1999).

[16] Parkins, A. S., and Walls, D. F., Phys. Rep. 303, 1(1998).

[17] A. J. Leggett, Rev. Mod. Phys. 73, 307 (2001).

[18] I. Bloch, J. Dalibard, W. Zwerger, Rev. Mod. Phys. 80, 885, (2008).

[19] C. Menotti, M. Lewenstein, arXiv:cond-mat/0711.3406.

[20] S. Yi and L. You, Phys. Rev. A 61, 041604 (2000).

[21] S. Yi and L. You, Phys. Rev. A 63, 053607 (2001).

[22] K. Goral, k. Rzazewski, and T. Pfau, Phys. Rev. A 61, p. 051601 (2000).

[23] A. Griesmaier, J. Werner, S. Hensler, J. Stuhler, and T. Pfau, Phys. Rev. Lett. 94, p. 160401 (2005).

[24] C. Ospelkaus, S. Ospelkaus, L. Humbert, P. Ernst, K. Sengstock, K. Bongs, Phys. Rev. Lett. 97, p. 120402 (2006).

[25] L. Santos and T. Pfau, Phys. Rev. Lett. 96, 190404 (2006).

[26] Springborg, M., "Methods of electronic structure calculations", (John Wiley&Sons, New York, 2000).

[27] Arfken, G., "Mathematical Methods for Physicists", (Orlando, FL: Academic Press, 1985).

[28] Fetter, A., L., Walecka, J., D., "Quantum Theory of Many-Particle Systems", (McGraw-Hill Hill Publishing Company, 1971).

[29] MathWorld–A Wolfram Web Resource, http://mathworld.wolfram.com/Sphere-SphereIntersection.html, Accessed: 15.06.2009.